

FLOW FIELD ANALYSIS OF CENTRIFUGAL PUMP BASED ON LARGE EDDY SIMULATION

F. QI¹ G. LIU¹ A. HORIA² G. LIU³ G. LI¹

Abstract: *Pump is a common machine in the building industry and water supply and drainage industry. The reasonable selection of the pump has a positive effect on the production efficiency. The IHF150-125-250 centrifugal pump was used as the reference object for 3D modeling in this paper. Firstly, the "simulation-experiment" method was used to verify the rationality of the flow field simulation of the six-blade centrifugal pump based on large eddy simulation (LES). Then the influence of different blade numbers on flow field was studied in detail. LES based on discrete phase model can obtain many flow field microstructures and flow images that cannot be obtained by the Reynolds-averaged Navier-stokes (RANS) method based on multi-fluid model. The simulation results showed that the excessive number of centrifugal pump blades would increase the friction of the blade surface, which reduced the total power at the outlet of the centrifugal pump, thus the head and efficiency of the centrifugal pump was reduced. Through simulation experiments, it was founded that when the number of blades was 5, the centrifugal pump flow field had the best comprehensive performance, lower turbulence intensity, the highest efficiency and best flow field stability.*

Key words: *centrifugal pump; large eddy simulation; flow field; number of blades; building industry*

1. Introduction

Centrifugal pumps are important energy conversion and fluid transfer devices. Their performance is essentially reflected in the internal flow field and is widely used in industrial, agricultural and aerospace applications. With the development of the global economy and the continuous improvement of the technical level of the civil centrifugal pump manufacturing process, the rapid development of the downstream civil fields such as municipal engineering, farmland and water conservancy, building and water supply and drainage projects has promoted the expansion of the application of civil centrifugal pumps, and its demand has increased year by year. Therefore, improving the operating efficiency, extending the service life, improving the stability of the fluid inside the

¹ Faculty of Mechanical Engineering, *Shenyang Jianzhu* University, China.

² Automotive Laboratory, *Transilvania* University of Braşov.

³ Caofeidian Holding Co., Ltd., China.

centrifugal pump and improving the safety of the operation of the centrifugal pump are urgent problems to be solved in the field of building. Numerical simulation is one of the important means to optimize centrifugal pumps. Many scholars have studied it [4, 8]. Some scholars [3] have used this method to study the flow field performance of the centrifugal pump. Since RANS method requires meshing of the boundaries, the fineness of the mesh affect the simulation results, and the change of the vortex shape has a great influence on the results [1, 9]. LES can obtain more and more detailed flow information than RANS on eliminating the small-scale vortex [7]. Therefore, LES becomes more and more advantageous [2].

In this paper, LES was used to simulate the full flow field of the centrifugal pump. The rationality of simulation data was verified by experiments. The relative velocity distribution and static pressure distribution of flow field were shown. The influence of the number of blades on the worm gear cover of the centrifugal pump on the distribution of the inner flow field was analysed.

2. Simulation Model

In this paper, the IHF150-125-250 fluoroplastic centrifugal pump was used as the reference object. The number of blades ranged from 3 to 8 in this numerical analysis. Figure 1 is the three-dimensional model of a twisted six-blade worm gear cover. Figure 2 is a three-dimensional model of the volute water body.

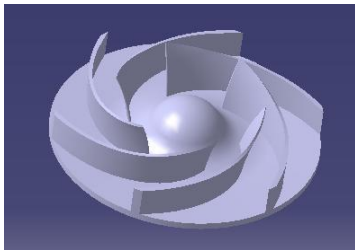


Fig. 1. 3D model of worm gear cover



Fig. 2. 3D model of volute water body

3. Simulation Method

The simulation method of this paper adopted Large Eddy Simulation (LES). The simulation idea is that direct simulation is used to simulate large-scale turbulent motion, and the sub-grid scale model is used to simulate the influence of small-scale turbulent motion on large-scale turbulent motion. The large eddy simulation equations were filtered and improved on the basis of Reynolds-averaged Navier-stokes (RANS) equations, and the optimal equations of LES were obtained.

The models of different flow rates were simulated. The worm gear rotates was 1450rot/min. LES do not require manual mesh division, which is closer to direct numerical simulation. For its condition setting, the inlet boundary used velocity inflow and the outlet boundary used free flow.

3.1. Control equation

The common three-dimensional compressible N-S equations consist of three sets of equations: momentum equations of three velocity components, mass equations, and energy equations. N-S equations were filtered in this paper and obtained the control equations of LES: continuous equation, energy equation and momentum equation.

Continuous equation:

$$\frac{\partial \bar{\rho}}{\partial t} + \frac{\partial (\bar{\rho} \hat{u}_j)}{\partial x_j} = 0 \quad (1)$$

and,

$$\begin{aligned} \hat{\rho} u_i u_j &= \bar{\rho} \hat{u}_i \hat{u}_j = \bar{\rho} (\hat{u}_i \hat{u}_j + \hat{u}_i u_j - \hat{u}_i \hat{u}_j) \\ \hat{\rho} u_i u_j &= \bar{\rho} \hat{u}_i \hat{u}_j + \bar{\rho} (\hat{u}_i u_j - \hat{u}_i \hat{u}_j) \end{aligned} \quad (2)$$

In the formula (2), $\tau_{ij} = \bar{\rho} (\hat{u}_i u_j - \hat{u}_i \hat{u}_j)$ is sub-grid stress.

Energy equation:

$$\frac{\partial (\bar{\rho} \tilde{e})}{\partial t} + \frac{\partial [(\bar{\rho} \tilde{e} + (\gamma - 1) M r^2 \bar{p}) \hat{u}_j]}{\partial x_j} = \frac{\partial}{\partial x_j} \left[\frac{+(\gamma - 1) M r^2}{Re} \hat{\sigma}_{jk} \hat{u}_k - \frac{1}{Re} (\hat{q}_j + q_j^{SGS}) \right] \quad (3)$$

In the formula (4), $q_j^{SGS} = -\frac{\mu^{SGS}}{Pr_t} \frac{\partial T}{\partial x_j}$ is sub-grid heat.

Momentum equation:

$$\frac{\partial}{\partial t} (\bar{\rho} \hat{u}_i) + \frac{\partial}{\partial x_j} (\bar{\rho} \hat{u}_i \hat{u}_j + \bar{p} \delta_{ij}) = \frac{1}{Re} \frac{\partial \hat{\sigma}_{ij}}{\partial x_j} - \frac{\partial \tau_{ij}}{\partial x_j} \quad (4)$$

In these formula, \tilde{e} is the total energy of each control body, ρ is the density, Re is the Reynolds number, γ is the specific heat ratio (adiabatic index), P is the pressure, u is the velocity component, σ is the normal stress, τ is the shear stress, M is the Mach number, T is the temperature and μ is the viscosity of the fluid.

4. Verification of Simulation Rationality

The accuracy of the simulation needs to be verified before detailed simulation. Due to the limitations of the equipment, the accuracy of the simulation of the centrifugal pump of the six-blade worm wheel was only verified by the "simulation-experiment" method. Comparing the experimental data under the same working conditions, when the simulation data is within the allowable range of error, the simulation data is proved to be reasonable and accurate.

Figure 3 is the velocity vector diagram and static pressure diagram of the flow-path of the centrifugal pump under the rated flow of the clear water. It can be seen from the Figure 3(a): In the flow-path of the pump, the fluid flow rate of the impeller inlet area is the lowest compared with other areas of the flow-path. The velocity gradients in all directions are relatively small, so the hydraulic loss that occurs here is also small. When the fluid enters the impeller flow-path, its velocity is increasing until the fluid flows into the flow-path of volute

from the impeller outlet area. After the fluid enters the volute, it flows toward the volute outlet along the direction of impeller rotation. During this process, the velocity of the fluid is constantly decreasing. Although the impeller section is centrally symmetrical about the rotating shaft, its internal flow field is Non-central symmetry. So, the hydraulic loss of the pump increases. The velocity in the volute is relatively uniform except at the position near the volute tongue. When the fluid reaches the outlet area of the volute, the velocity is more uniform. It can be seen from Figure 3(b): After the fluid enters the impeller, the static pressure value is continuously increasing. After entering the volute from the impeller flow-path, the static pressure value is still increasing, but the increase is smaller. The increase of static pressure in the volute is mainly the conversion of kinetic energy to static pressure energy. The conversion of energy completes at the outlet area to maximize static pressure. From the analysis of the velocity vector field and the pressure field of the centrifugal pump, it can be seen that the numerical simulation results basically conform to the true flow of fluid of the centrifugal pump [5, 6].



(a). *Velocity Vector Diagram*

(b). *Static Pressure Diagram*

Fig. 3. *Absolute speed vector diagram and static pressure cloud diagram in the whole flow-path*

The rationality of the simulation is verified by comparison between simulation and experiment. Figure 4 is the comparison of H-Q under simulated and experimental conditions. It can be seen from Figure 4: The head deviation is less than 3% when the flow rate is greater than 400m³h⁻¹. The head deviation is not more than 5% under all flow rate conditions. All errors are within the tolerances.

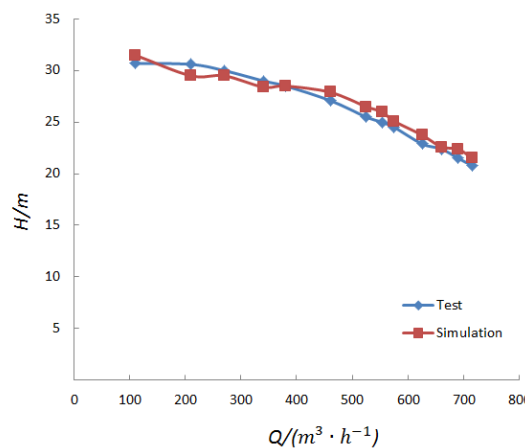


Fig. 4 *H-Q comparison curves ($n=1\ 450\ r \cdot min^{-1}$)*

Therefore, through the analysis of velocity vector diagram and static pressure diagram and the comparison between simulation and experiments, the simulation data is effective and reliable, and detailed data processing and analysis can be performed.

5. Analysis of Simulation Result

The impeller is the core component of the centrifugal pump. It is most influential for the form of fluid motion and the state of flow field of the centrifugal pump by the shape of impeller and the form of motion. Therefore, combining the velocity field and the static pressure field to analyse the flow condition of the pump is of great significance for the optimal design and efficient operation of the pump.

5.1. H-Q characteristic analysis of centrifugal pump

Figure 5 is the H-Q comparison curves of centrifugal pump of different blade number. Overall, the trend of head curves of different blades is similar, but the values of the heads are quite different. At small flows, the flow has less effect on the head and the slope of the curve is flatter. At the design flow rate, the heads of blades 5 to 8 have a positive slope instead. At large flow rates, the slope changes rapidly, and the head value of blades 7 is smaller than the blade 5 or 6. The reason is that in the centrifugal pump of the blades 3 to 5, the work done by the fluid is greater than the energy loss of friction by the blade surface and the volute. When the number of blades is 5 or 6, the positive work done by the liquid is basically consistent with the loss of friction.

Therefore, the total energy and the head value are basically unchanged in this interval. When the number of blades is 6 to 8, the total surface area of the blades increases due to the increase in the number of blades, and the friction loss is greater than the positive work done by the fluid. Therefore, the total energy decreases with the number of blades in this interval, resulting in a decrease in the head.

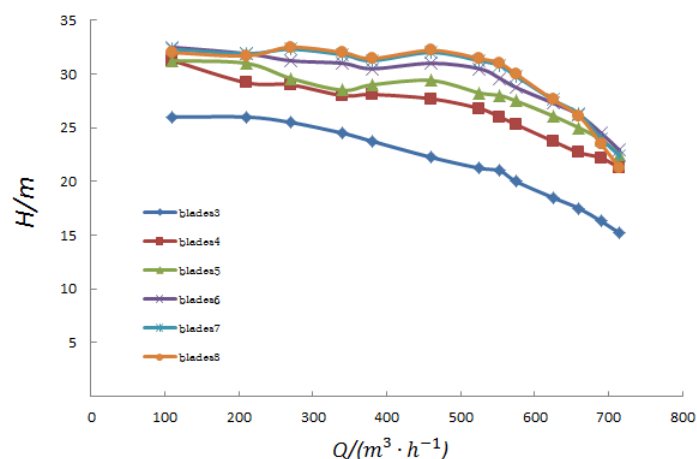


Fig. 5. Centrifugal pump H-Q comparison curves of different blade numbers ($n=1450 \text{ r} \cdot \text{min}^{-1}$)

5.2. Analysis of flow pressure distribution of centrifugal pump

Figure 6 is the pressure distribution on the centre plane of flow-path of the centrifugal pump of different blade number. In the figure, Z is the number of blades. It can be seen from Figure 6: there is a low pressure zone in the suction surface area, which is a region prone to cavitation. The flow field of all number of blades has a low pressure zone. But in comparison, the flow field of Z=5 or 6 has a relatively smaller area of low pressure zone and the low pressure is lighter.

The low pressure of flow field of Z=4 is heavier, and the negative pressure is larger, so cavitation is more likely to occur here. The low pressure zone of flow field of Z=7 or 8 is larger, and the low pressure is heavier, so cavitation is also more likely to occur. The low pressure zone at the impeller inlet is generated as the fluid accelerates through the head of blades, the flow rate is increased, and the fluid at the inlet is reduced. Then, due to the rotation of the impeller, the water flow in the impeller path gradually increases with the increase of the radius, and the pressure gradually increases. At the same time, as Z increases, the area of the low pressure zone also increases.

So the number of blades has a certain influence on the cavitation of the centrifugal pump. As Z increases, the pressure distribution of the impeller flow-path is improved, but Z is not as good as possible. When Z is 5, the pressure difference between the pressure surface and the suction surface in the flow-path is small, the adverse pressure gradient is moderate, and the flow performance is relatively good.

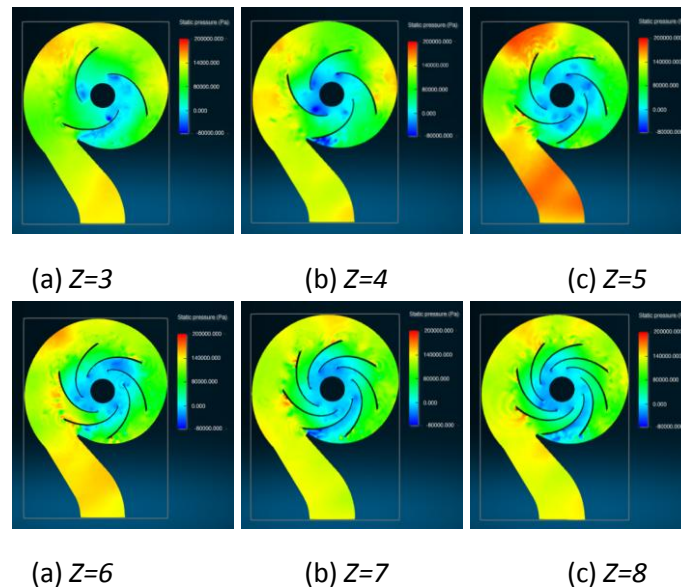


Fig. 6. The pressure distribution on the centre plane of different blades

5.3. Analysis of flow velocity distribution of centrifugal pump

Figure 7 is the velocity distribution on the centre plane of flow-path of the centrifugal pump of different blade number. The smoother the change of velocity from the pressure surface to

the suction surface, the more stable the flow. It can be seen from Figure 7: when Z is 7 or 8, the velocity from the pressure surface to the suction surface changes obviously, indicating that the flow is relatively unstable.

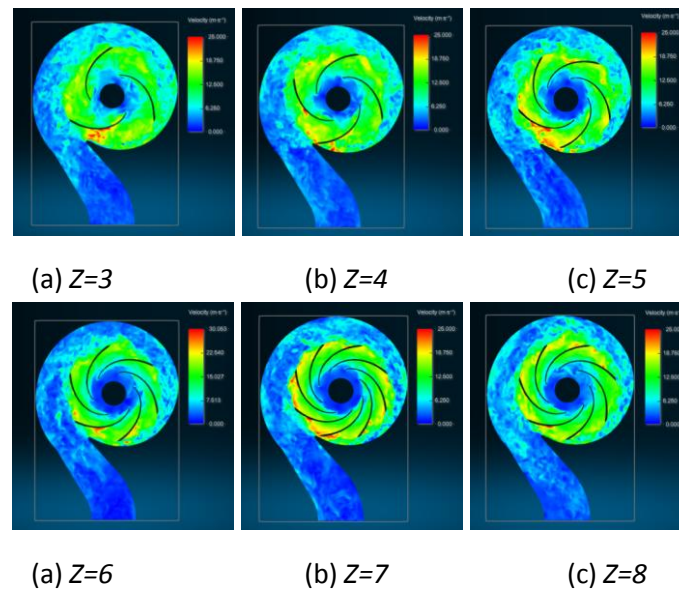


Fig. 7. The velocity distribution on the centre plane of different blades

Obvious jet-wake phenomenon can be seen near the volute tongue with $Z=3, 4$ or 5 . However, the jet-wake phenomenon is not obvious in the flow-path with $Z= 6, 7$ or 8 . Increased Z can help reduce jet-wake losses. However, when Z is too large, the relative velocity changes more obviously from the pressure surface to the suction surface.

6. Conclusion

This simulation obtains the parameter distribution and the vorticity distribution of the full flow field.

The H - Q characteristics and η - Q characteristics of the six-blade impeller centrifugal pump obtained by the simulation are in good agreement with the experimental results. The main conclusions are as follows:

- as the number of blades increases, the pressure difference between the pressure surface and the suction surface decreases, and the jet-wake phenomenon in the flow-path also improves. When the number of blades is greater than 5, the internal losses of the flow-path increase correspondingly as the number of flow-path increases.
- the centrifugal pump studied in this paper has the highest efficiency and stable working area when the number of blades is 5 under large flow. However, at small flow rates, the influence of the number of blades on the flow field is not significant. The results of this study provide a reference for revealing the mechanism of complex

flow phenomena of centrifugal pumps.

It has a guiding role in improving the operating efficiency, extending the service life, improving the stability of the fluid inside the centrifugal pump and improving the safety of the operation of the centrifugal pump in the field of building.

References

1. Guo, Y., Yuan S., Luo, W., et al.: *Unsteady characteristics of water torque of centrifugal pump blades based on CFD*. In: Journal of Drainage and Irrigation Machinery Engineering (2016) Vol. 34 (6), p. 470-476.
2. Hang, H., Son, G.: *Direct numerical simulation of 3D particle motion in an evaporating liquid film*. In: Journal of Mechanical Science and Technology (2016) Vol. 30 (9), p. 3929-3934.
3. Liu, H., Wang, Y., Yuan, S., et al.: *Effects of blades number on characteristics of centrifugal pumps*. In: Chinese Journal of Mechanical Engineering (2010) Vol. 23, p. 1-6.
4. Tan, L., Cao, S.: *Optimal design and numerical simulation for impeller of centrifugal pump with medium-high specific speed*. In: Journal of Drainage and Irrigation Machinery Engineering (2010) Vol. 28 (4), p. 282-290.
5. Tan, M., Liu, H., Wang, Y., et al.: *CFD analysis of the influence of impeller outer diameter on the internal flow of centrifugal pump*. In: Drainage and Irrigation Machinery (2009) Vol. 27 (5), p. 314-318.
6. Tang, H., He, F.: *Numerical Simulation of Flow Field in Centrifugal Pump*. In: Pump Technology (2002) Vol. 3, p. 3-9.
7. Wang, L.: *Overview of large eddy simulation theory and its application*. In: Journal of Hohai University (Natural Science), 2004, p. 261-265.
8. Wang, X., Wang, C., LI, Y.: *Numerical study of flow characteristics in the impeller side chamber of centrifugal pump*. In: Transactions of the Chinese Society for Agriculture Machinery (2009) Vol. 40 (4), p. 86-90.
9. Wang Y, Wang, Z., Chen C., et al.: *Numerical simulation of cavitation flow field of centrifugal pump based on Fluent*. In: Journal of Agricultural Mechanization Research (2012) Vol. 34 (11), p. 59-63.